GPR120 Prevents Colorectal Adenocarcinoma Progression by Sustaining The Mucosal Barrier Integrity

Federica Rubbino
Humanitas Clinical and Research Center – IRCCS
Valentina Garlatti
Università degli studi del Piemonte Orientale “Amedeo Avogadro”
Valeria Garzarelli
CNR NanoTec
Luca Massimino
Humanitas University
Salvatore Spanò
Humanitas University
Paolo Iadarola
University of Pavia
Maddalena Cagnone
Labanalysis L.L.C
Martin Giera
Leiden University Medical Center
Marieke Heijink
Leiden University Medical Center
Simone Guglielmetti
Università degli studi di Milano
Vincenzo Arena
Fondazione Policlinico Universitario Agostino Gemelli, IRCCS Università Cattolica del Sacro Cuore
Alberto Malesci
Humanitas University
Luigi Laghi
Humanitas Clinical and Research Center, IRCCS
Silvio Danese
Humanitas University
Stefania Stefania Vetrano (Stefania.vetrano@hunimed.eu)
Humanitas University

Research Article

Keywords: GPR120, Colorectal cancer, epithelium, microbiota, intestinal permeability

Posted Date: June 15th, 2021

DOI: https://doi.org/10.21203/rs.3.rs-598555/v1

Version of Record: A version of this preprint was published at Scientific Reports on January 10th, 2022.
See the published version at https://doi.org/10.1038/s41598-021-03787-7.

GPR120 prevents colorectal adenocarcinoma progression by sustaining the mucosal barrier integrity

Federica Rubbino[1], Valentina Garlatti[2], Valeria Garzarelli[3], Luca Massimino[4], Salvatore Spanò[4], Paolo Iadarola[5], Maddalena Cagnone[6], Martin Giera[7], Marieke Heijink[7], Simone Guglielmetti[8], Vincenzo Arena[9], Alberto Malesci[4,10], Luigi Laghi[10,11], Silvio Danese[4,12] & Stefania Vetrano*[4,12]

[1]Humanitas Clinical and Research Center – IRCCS, Dept. of Gastroenterology - Laboratory of Molecular Gastroenterology, Rozzano (Milan), Italy

[2] Department of Pharmaceutical Science, Università degli studi del Piemonte Orientale "Amedeo Avogadro", Novara, Italy

[3] Institute of Nanotechnology, CNR NanoTec, Lecce, Italy

[4]Department of Biomedical Sciences, Humanitas University, Pieve Emanuele (Milan), Italy

[5] Department of Biology and Biotechnology "L. Spallanzani", University of Pavia, Italy

[6] Labanalysis L.L.C. , Casanova Lonati, Pavia, Italy

[7] Center for Proteomics and Metabolomics, Leiden University Medical Center, Leiden, The Netherlands

[8] Division of Food Microbiology and Bioprocesses, Department of Food Environmental and Nutritional Sciences (DeFENS), Università degli studi di Milano, Milano, Italy.

[9]Fondazione Policlinico Universitario Agostino Gemelli, IRCCS Università Cattolica del Sacro Cuore, Roma, Italy.

[10]Humanitas Clinical and Research Center, IRCCS, Dept. of Gastroenterology, Rozzano (Milan), Italy

[11] University of Parma, Department of Medicine and Surgery, Parma, Italy

[12]IBD Center, Laboratory of Gastrointestinal Immunopathology, Humanitas Clinical and Research Center-IRCCS, Rozzano (Milan), Italy

*Correspondence to: Stefania Stefania Vetrano, PhD
Assistant professor in Applied Biology
Humanitas University
Via Rita levi Montalcini
Pieve Emanuele (Milan) Italy
Stefania.vetrano@hunimed.eu

Abstract

Background&Aims: GPR120 (encoded by *FFAR4* gene) is a receptor for long chain fatty acids, activated by ω-3 PUFAs, and expressed in many cell types. Its role in the context of colorectal cancer (CRC) is still puzzling with many controversial evidences. Here, we explored the involvement of epithelial GPR120 in the CRC development.

Methods: Both *in vitro* and *in vivo* experiments were conducted to mimic the conditional deletion of the receptor from gut epithelium. Intestinal permeability and integrity of mucus layer were assessed by using Evans blue dye and immunofluorescence for MUC-2 protein, respectively. Microbiota composition, presence of lipid mediators and short chain fatty acids were analyzed in the stools of conditional GPR120 and wild type (WT) mice. Incidence and grade of tumors were evaluated in all groups of mice before and after colitis-associated cancer. Finally, GPR120 expression was analyzed in 9 human normal tissues, 9 adenomas, and 17 primary adenocarcinomas.

Results: Our work for the first time highlight the role of the receptor in the progression of colorectal cancer. We observed that the loss of epithelial GPR120 in the gut results into increased intestinal permeability, microbiota translocation and dysbiosis, which turns into hyperproliferation of epithelial cells, likely through the activation of β -catenin signaling. Therefore, the loss of GPR120 represents an early event of CRC, but avoid its progression as invasive cancer.

Conclusion: these results demonstrate that the epithelial GPR120 receptor is essential to maintain the mucosal barrier integrity and to prevent CRC developing. Therefore, our data pave the way to GPR120 as an useful marker for the phenotypic characterization of CRC lesions and as new potential target for CRC prevention.

Keywords: GPR120; Colorectal cancer; epithelium; microbiota; intestinal permeability

Introduction (443 words)

G protein-couple receptors (GPCRs) are responsible for the signal transduction of a wide variety of ligands, including hormones, growth factors, and lipids[1,2] mediating several cellular processes, and so have great potential as therapeutic targets for a broad spectrum of diseases including tumor[3]. GPR120, also named free fatty acid (FAs) receptor-4 (*FFAR4*), the receptor for long-chain fatty acids, activated by n3 Polyunsaturated Fatty Acids (ω-3 PUFA)[4,5], mediates insulin sensitizing and anti-diabetic effects by repressing macrophage-induced tissue inflammation playing a key role in metabolic and inflammatory diseases. However, GPR120 is expressed also in several cell types, including the intestinal epithelial cells[6,7], where seems to exert anti-inflammatory effects once activated by PUFAs[4,8]. In tumors, GPR120 expression positively correlated with clinical response to chemotherapy in patient with breast cancer[9] and its activation promotes metastasis in lung tissue through PI3K/Akt/NF-KB signaling[10] . Increased level is detected in esophageal cancer, in which its expression positively correlates with tumor progression[11]. In prostate cancer cell-lines, GPR120 promotes the anti-cancer effects of ω-3 PUFAs by blocking ERK1/2 signaling pathway and cell proliferation, migration and survival[12]. On the other side, activation of GPR120 by selective agonists may exacerbate the malignant phenotype of pancreatic cancer cell lines[13]. Its expression positively correlated with advanced tumor stage in colorectal cancer (CRC) patients[14]. Although some evidences showed that GPR120 enhances angiogenesis and dissemination promoting epithelial-to-mesenchymal transition (EMT)[15], GPR120 function in colorectal cancer development is still puzzling.

Despite the advances in screening and surveillance, CRC remains the second most common cause of cancer death worldwide for which the molecular mechanisms driving the disease are still not clear. To date, is important to identify new potential molecules for tumor-preventive strategies. Here, we highlighted the functional role of GPR120 in the epithelial compartment and its involvement in the intestinal tumorigenesis providing evidence that the receptor contributes in the integrity of intestinal epithelial barrier. This barrier system, while avoiding harmful penetration, is selectively permeable to allow absorption of water and nutrients[16]. Thus, on the one hand it prevents the attachment and entry of pathogens into intestinal mucosa, and other hand cross-talks with the commensal microflora, which in turn contributes to the barrier by producing hydrosoluble and liposoluble vitamins [vitamin K, folate,] and short chain fatty acids (SCFAs)[17]. Emerging data demonstrate that defects of barrier function, as well as reduced mucus production, are early biological events in colorectal tumorigenesis, being crucial for the activation of underlining immune cells by microbial products[18–20]. We observed that GPR120 plays an important role in controlling intestinal homeostasis and restraining tumor

development. Our data highlight new activities exerted by GPR120 in CRC progression, and point at its potential role as a therapeutic target for CRC prevention.

Results (1610 words)

GPR120 is mainly expressed in gut epithelial cells.

Accordingly with other data[21], GPR120 is highly expressed by intestinal epithelial cells as demonstrated by the co-localization of the receptor with epithelial markers, such as cytokeratin (**Figure 1a, upper panel**) and junctional adhesion molecule A (Jam A) (**Figure 1a, lower panel**).

To determine its localization apical and basolateral side, we cultured the Caco-2 cells as 3-dimensional mini- organotypic allowing the polarization of epithelial cells and then we performed a staining with an apical marker, JAM-A. The co-localization of GPR120 with JAM-A pointed out the apical side localization of the receptor (**Figure 1b**).

GPR120 is involved in the maintenance of mucosal barrier integrity.

To explore the functional role of GPR120 on epithelial compartment, we generated mice with a conditional deletion of GPR120 on epithelial cells crossing GPR120flox/flox mice with *VillinCre* mice[22]. The GPR120 knockdown efficiency in the epithelial compartment was checked by immunofluorescence on colon tissues from both WT and GPR120$^{\Delta IEC}$ animals (**Figure 1c**).

Next, we explored the involvement of GPR120 in maintaining the integrity of mucosal barrier. To achieve this aim, we evaluated the intestinal permeability by perfusing the colonic mucosa of healthy GPR120$^{\Delta IEC}$ and WT littermates with Evans blue dye[23]. The assay revealed a significative increased dissemination of the dye into the mucosa of GPR120$^{\Delta IEC}$ compared to WT littermates (**Figure 1d**). This impairment was further confirmed by fluorescence in situ hybridization (FISH) of the colonic mucosa showing bacteria able to penetrate the MUC2 mucin-dependent mucus layer only of GPR120$^{\Delta IEC}$ mice (**Figure 1e**), Interestingly, the expression analysis of *MUC2* resulted significant reduced in healthy transgenic mice at gene and protein levels (**Figure 2a, b**) providing a clear evidence that GPR120 is involved in regulating permeability. To gain insight into the mechanisms underlying this function, we modulated the expression of GPR120 receptor *in vitro* in epithelial CRC cell lines Caco-2 cells and LoVo, both expressing high levels of GPR120 among the six cell lines analyzed (**Supplementary Figure 1a**).

After silencing of GPR120 using a specific siRNA (**Supplementary Figure 1b**), both cell lines were subjected to Transepithelial Electrical Resistance (TEER) measurement, showing a significant reduced resistance in both siRNA-treated cell lines (**Figure 1f, g**) than scramble controls, thus corroborating a role for GPR120 in maintaining mucosal barrier integrity.

Epithelial GPR120 deletion affects mucus and microbiota composition.

Since MUC2 expression was impaired in healthy GPR120 $^{\Delta IEC}$ mice (**Figure 2a, b**), we analyzed the protein composition of the mucus layer. The reconstruction of GPR120$^{\Delta IEC}$ and WT mucus samples, allowed the identification of 117 spots representing different proteins. Out of total spots, 29 were shared between GPR120$^{\Delta IEC}$ and WT mice, whereas 48 were detectable uniquely in WT and 40 uniquely in GPR120$^{\Delta IEC}$ mucus samples (**Figure 2c**). Correspondingly, we found clear differences in the mucus composition between the two experimental groups (**Figure 2d**). Among the proteins detected only in GPR120$^{\Delta IEC}$ mucus samples, Myosin 11 (Myh11), Myosin 9 (Myh9), and Vinculin (Vcl) which are related to mucosal barrier integrity were identified, strengthening the finding that the loss of the receptor in the intestinal epithelium affects mucus composition.

Next, we performed a microbiomic analysis by 16S rRNA gene profiling on faecal samples collected from healthy GPR120$^{\Delta IEC}$ and WT mice, in which no differences were detected in alpha- and beta-diversity comparisons between two groups (**Figure 2e, f**). A differential expression analysis based on the negative binomial distribution (DESeq2) allowed us to identify all differentially expressed operational taxonomic units (OTUs), with or without statistical significance (**Figure 2g**). Based on the taxonomic results, we found differences in the microbiota composition of GPR120$^{\Delta IEC}$ and WT mice even at steady state. In fact, we found 14 OTUs whose normalized relative abundance was significantly different between the two groups of mice (**Figure 2g**). In specific, 8 OTUs were overrepresented in mutant mice, including taxonomic units ascribed to the genus *Bacteroides* (1 OTU), the family S24-7 (3 OTUs), and, particularly, to the species *Akkermansia muciniphila* (4 OTUs) (**Figure 2h**). Conversely, 6 OTUs were overrepresented in WT mice, including taxonomic units ascribed to the genera *Adlercreutzia* and *Dehalobacterium*, and the families *Rikenellaceae*, S24-7 and *Ruminococcaceae* (**Figure 2h**). A fundamental role of microbiota is the production of SCFAs, for their trophic effects on intestinal epithelium[17]. Among the four major SCFAs produced as microbial metabolites –acetate, propionate, butyrate-and valeric acid- our results showed that only butyric acid was significantly upregulated in transgenic mice in healthy condition (**Figure 2i**).

GPR120 attenuates tumorigenesis during inflammation-driven colorectal cancer.

Emerging data demonstrate that defects of barrier function, as well as reduced mucus production, are early biological events in colorectal tumorigenesis. Hence, it was important to investigate whether GPR120 deficiency leads to more severe colitis-associated cancer (CAC). To verify that, GPR120$^{\Delta IEC}$ and WT mice were subjected to the azoxymethane (AOM)/dextran sodium sulfate (DSS)-induced model of colitis-associated CRC (**Figure 3a**). Results revealed no significant differences in clinical signs of intestinal inflammation between GPR120$^{\Delta IEC}$ and WT mice, as shown by comparable body

weight loss (**Supplementary Figure 2a**), and DAI score (**Supplementary Figure 2b**) throughout the entire experiment.

Tumor growth was quantified by colonoscopy at the termination end point (**Figure 3b**) as described previously[24]. Transgenic mice showed a significant increase of tumor density along the colon in comparison to WT animals (**Figure 3c**). Furthermore, the histological analysis of the colon tissue revealed that tumor lesions in GPR120$^{\Delta IEC}$ mice were characterized by a higher number of small-sized tumors (**Figure 3d**). This finding was consistent with a significantly higher number of proliferating cells in colons from GPR120$^{\Delta IEC}$ mice, as shown by immunohistochemical staining for the proliferative marker Ki67 (**Figure 3e, f**). While both wild-type and transgenic mice developed low- and-high grade adenomas (**Figure 3g, left and center panels**), strikingly GPR120 $^{\Delta IEC}$ mice did never develop any adenocarcinoma (**Figure 3g, right panel**). This finding suggests that epithelial GPR120 is crucial in the early event of dysplastic lesions rather than progression.

GPR120 expression is reduced in human adenocarcinoma.

Given the loss of epithelial GPR120 results in increased adenoma incidence in mouse model, we explored its expression in a retrospective cohort of human adenomas and adenocarcinomas. We found that the expression of *FFAR4* gene decreases increasing the grade of the lesion (**Figure 4a**). More specifically, the expression of the receptor is significantly downregulated in adenocarcinomas compared to healthy colon, as well as compared to adenomas. This was confirmed at protein level by immunostaining (**Figure 4b and c**), in which the expression of GPR120 was significantly higher in High Grade Adenoma (HGA), compared to stage 1 and 2 tumors (T1 and T2). Importantly, GPR120 expression was drastically reduced in the epithelium (**Supplementary Figure 3**) and detectable on immune infiltrate. Additionally, *in silico* analysis performed by using Gene Expression Across Normal and Tumor tissue (GENT2) database, revealed *FFAR4* significantly downregulated in CRC tissues when compared to healthy controls (**Figure 4d**). All these human evidences support the hypothesis that epithelial GPR120 is not only involved in the early stage of CRC, but it also has a role in the progression.

GPR120 modulation impacts epithelial cell proliferation.

To better investigate the role of GPR120 in epithelial cell proliferation (**Figure 3e, f**), we explored the effects of GPR120 silencing on human cancer cells lines. Both siRNA-treated Caco2 and LoVo cells displayed an increased number of proliferative cells in comparison with their relative controls (**Figure 5a, left and right panel respectively**). Then, we performed both cell cycle analysis and apoptosis detection on siRNA-treated and scramble control cells. Both Caco-2 and LoVo siRNA

silenced cells showed a higher percentage (30% more) of cells in G1 phase (**Figure 5b, left and right panel respectively**), while the percentage of apoptotic cells was comparable in both groups (**Supplementary Figure 4a, b**). Of note, the gene encoding for Cyclin D1, promoter for G1-to-S transition, was even significantly up-regulated in siRNA treated cells (**Figure 5c**). As some evidences reported that GPR120 regulates cell proliferation modulating intracellular levels of Ca^{2+} [25,26], we measured its levels after GPR120 silencing. Results showed no differences in the concentration of intracellular Ca^{2+} between siRNA-treated Caco-2 and LoVo cells and their relative scramble siRNA-treated controls (**Figure 5d**), indicating that GPR120 does not affect proliferation of CRC cells by modulation of Ca^{2+} influx. From our functional enrichment analysis on DEGs in the RNAseq, performed on epithelial cells isolated from healthy wild-type and transgenic mice, we observed biological processes related to Wnt pathway signaling to be the most significantly enriched in GPR120$^{\Delta IEC}$ compared to WT epithelium. This pathway is known to be involved in cell growth, differentiation, and apoptosis and one of its key mediators is represented by β-catenin[27].

A deeper analysis showed indeed a significative upregulation of *Ctnnb1,* the gene encoding for β-catenin, in the epithelium of GPR120$^{\Delta IEC}$ healthy mice compared to WT (**Figure 5e**). Interestingly, this data was confirmed not only in tumor bearing GPR120$^{\Delta IEC}$ animals versus WT, as shown by qRT-PCR (**Figure 5f**), and immunohistochemical analysis on colon sections from AOM/DSS- treated mice (**Figure 5g, h**), but also on Caco-2 and LoVo cells, upon GPR120 silencing (**Figure 5i**), suggesting that GPR120 may directly affect CRC cell proliferation through β-catenin signaling.

Epithelial GPR120 influences the fecal lipidomic profile of AOM/DSS treated mice.

Since the ω-3 polyunsaturated fatty acids (PUFAs), docosahexaenoic acid (DHA) and eicosapentaenoic acid (EPA) are established activators of GPR120[5], and a current body of literature supports their beneficial effects in the context of CRC, we analyzed the lipidomic profile in healthy and tumor-bearing mice. Results showed that while no differences were evident in the amount of ω-6 PUFAs between GPR120 $^{\Delta IEC}$ and WT mice at any time point (**Supplementary Figure 5a**), among ω-3 PUFAs a significant downregulation of DHA was apparent at each time point in GPR120$^{\Delta IEC}$ mice compared to WT (**Figure 6a**). Among DHA-derived lipid mediators, we found a significant reduction of 17-HDHA both at 4 and 8 weeks in transgenic mice versus WT (**Figure 6b**), and the 7-HDHA downregulated only at 8 weeks (**Figure 6b**). The downregulation of these specific lipid mediators in transgenic animals was not due to a reduced expression of the genes encoding for their enzymes (15-LOX and 5- LOX respectively), named *Alox15A* and *Alox15B*, as shown by qRT-PCR (**Supplementary Figure 5b**).

Discussion

Our study demonstrates that epithelial GPR120 plays an essential role in maintaining mucosal barrier integrity, and in preventing the inappropriate bacteria recognition and penetration that are linked to cancer development[28]. In this context, the inner mucus layer plays a crucial role in defending host against pathogens[29]. However, we are still only at the beginning of understanding the mechanism by which the integrity of the inner mucus layer is maintained by the host, particularly when challenged with microorganism penetration.

Gut epithelial cells are efficiently protected by the mucus, mainly - but not only -consisting of mucin 2 (Muc2)[30]. The mucus is composed of two distinct layers: an inner mucus layer firmly attached to the epithelium, and an outer non-attached layer, easy to remove[31,32], and besides mucins, it is characterized by other proteins that help to maintain the epithelial barrier integrity[32]. Our proteomic analysis performed on the mucus of healthy GPR120$^{\Delta IEC}$ mice and WT littermates revealed interesting differences in the mucus composition of the two groups. Among the proteins found expressed in both groups, we observed Muc2 to be significantly downregulated in healthy GPR120$^{\Delta IEC}$ than WT littermates. This is important, because downregulation of Muc2 expression was associated with early carcinogenesis events in colon cancer[33,34], which is consistent with the fact that at later stages of CRC development no differences in colonic *Muc2* levels were observed between tumor bearing GPR120$^{\Delta IEC}$ and WT mice (data not shown).

Among proteins that were exclusively present in the mucus of GPR120$^{\Delta IEC}$ mice, worthy of attention are Myosin 11 (Myh11), Myosin 9 (Myh9), and Vinculin (Vcl). In fact, myosins are essential regulators of cellular homeostasis and tissue integrity, playing multiple roles in cell polarity, division, motility, and mechanotransduction; some of them have been shown to play important roles in establishing normal intestinal barrier, and protection from mucosal inflammation *in vivo*[35]. A study from Wallace and colleagues showed that Myh11 mutation disrupts epithelial architecture in the developing zebrafish intestine, interfering with cells integrity and inducing epithelial cells to acquire an invasive phenotype[36]. Furthermore, Myh6 and vinculin are part of a molecular apparatus responsible for generating the cohesive cell–cell contacts that distinguish epithelial biogenesis *in vitro*[37]. On the other hand, Vinculin is reported to be involved in pathogenic bacteria invasion, a phenomenon well characterized for Gram-negative *Shigella*, but less known for other bacterial species[38]. These proteins, together with the up-regulation of some SCFAs, could explain why epithelial deletion of GPR120 did not affect intestinal inflammation. Small Chain Fatty Acids produced as microbial metabolites, namely acetate, propionate, and butyrate, can modulate many biological responses like inflammation, through two mechanisms; while one is associated with the inhibition of nuclear class I histone deacetylases (HDACs), the other acts through the direct activation

of some G-protein coupled receptors (GPCRs)[39]. Among SCFAs, butyric acid is the only one stands out as upregulated in transgenic mice, and it is extensively studied for its controversial effect named as "butyrate paradox", in which a wealth of experimental evidence has demonstrated the inhibitory effect of butyrate on tumorigenesis[40] and the capacity to mediate anti-inflammatory effects[41], but this SCFA can also paradoxically stimulate mucosal proliferation under certain conditions[42].

In parallel, we observed changes in the intestinal microbiota of healthy and AOM/DSS-induced GPR120$^{\Delta IEC}$ versus WT animals, whose alteration may either be the cause or the consequence of the altered mucus composition. To date, there is no consensus on the composition of the gut microbiota in preneoplastic lesions or CRC. However, some bacterial species such as *Bacteroides fragilis*, and *Escherichia coli*, have been correlated with CRC carcinogenesis[43]. Among the bacteria significantly more abundant in healthy GPR120$^{\Delta IEC}$ versus WT animals, we found an OUT belonging to the genus *Bacteroides*. Members of this bacterial taxon have been recognized among the "drivers" of CRC, and their metabolites can damage the DNA of colonic epithelium, leading to initiation of tumor development[43], which is consistent with the increased susceptibility of GPR120$^{\Delta IEC}$ mice to the AOM/DSS protocol. The higher abundance of *Akkermansia muciniphila* in healthy GPR120$^{\Delta IEC}$ versus WT animals, is also intriguing; in fact, *A. muciniphila* is a Gram-negative and anaerobic bacterium, that colonizes the intestinal mucus layer[45]. This bacterium is able to degrade host mucin into various products (e.g., short chain fatty acids) to regulate host biological functions, such as glucose and lipid metabolism, and to modulate the expression of mucus-related genes, which participate in host immune responses[45]. *A. muciniphila* was confirmed to exert a major role in maintaining gut barrier function, host metabolism and other biological functions through interactions between intestinal microbes and host in metabolic disorders[46]. All these notions support and sustain our hypothesis that epithelial deletion of GPR120 is important to maintain the mucosal barrier integrity, and the resemblances observed in the parameters for the inflammation derived from these mechanisms of compensation.

The role of the receptor in CRC is still unclear. Wu and colleagues found that the expression of *FFAR4,* the gene encoding for GPR120, is upregulated in human CRC tissue compared to adjacent non-cancerous areas[14], and that the expression of the receptor increases as the clinical stage of advanced cancer. In sharp contrast, Zhang and colleagues demonstrated that GPR120 suppresses cell proliferation and promotes apoptosis in CRC cells treated with ω-3 PUFA[47]. Our findings demonstrate that *FFAR4* is significantly downregulated in human CRC by using the GENT2 database, but also that the expression of the receptor decreases increasing the grade of lesion as invasive cancer, and then additional evidence rise up from *in vivo* model in which conditional deletion of GPR120 in

the intestinal epithelium significantly increased the density of small-sized lesions, as well as encourage the absence of malignant lesions. This was consistent with a significantly higher number of proliferating cells in colon from AOM/DSS-induced transgenic mice, as shown by immunohistochemical staining for the proliferative marker Ki67, and the proliferation assay *in vitro* upon GPR120 siRNA silencing, indicating that epithelial GPR120 in the gut promotes CRC growth but not progression. Wnt signaling pathway, whose dysregulation may lead to tumor development and growth[48], was found altered in absence of GPR120. Biological processes related to the Wnt pathway have been indeed found enriched in the epithelium of healthy GPR120$^{\Delta IEC}$ versus WT mice. In addition, *CTNNB1* gene, was significantly up-regulated in siRNA treated cells. Furthermore, we did not observe any nuclear β-catenin localization, with most of its expression localized in the cytoplasm of intestinal epithelial cells. On the basis of what published by Wong and others[49–51], our results are consistent with the lack of differences between GPR120$^{\Delta IEC}$ and WT mice in the number of low- and high-grade adenomas, and with the significantly higher number of small-sized tumoral lesions in GPR120$^{\Delta IEC}$ versus WT animals, but the adenocarcinoma were absent only in GPR120$^{\Delta IEC}$ animals. Most likely, the β-catenin accumulation outcome from the absence of the receptor in the gut epithelium allowing the hyperproliferation. However, a deeper investigation about the role of GPR120 in cancer progression is needed.

Worthy of interest is our evidences showing that epithelial GPR120 is important to slow down the cancer progression. In this context the contribution of ω-3 PUFAs may make the difference. Many clinical studies have confirmed the inverse correlation between CRC and ω-3 PUFAs intake[52–54]. Consistently with that, our results showed a down-regulation of ω-3 PUFAs, and it is even in line with evidences in which high ratio ω-3-derived lipids may be considered as biomarker promoting for metastatic CRC[55]. The previous studies showed that CRC cells preferentially uptake ω-3 PUFAs[56], and that a correlation between the expression receptors and its ligands[57] is possible. Taken together with our findings, in which the absence of the receptor is associated with ligands' downregulation, we strongly believe in a possible autocrine loop, with consequent reduction of these lipids the uptake is not possible and then cancerous cells cannot progress as invasive cancer. Finally, the ω-3 PUFAs have even effects on intestinal permeability: EPA and DHA have been shown to improve barrier integrity in *in vitro* studies[58]. Moreover, many studies support the role of EPA and DHA as modifier of proliferative pattern in epithelial cells in patients with sporadic adenomatous polyps, but the mechanism exerting this effect in colonic mucosa is not clear yet[59].

In conclusion, in the present study we provided for the first-time evidences of the epithelial GPR120 role in maintaining the protective inner mucus layer. Its loss promotes epithelial barrier impairment

dysbiosis and bacterial translocation, and hyperproliferation of epithelial cells, but on the other hand prevents tumor progression. Although, further studies are needed to elucidate better the molecular involvement of GPR120, our data pave the way to future applications of GPR120 as an useful marker in clinics.

Materials and methods

Animal studies: In order to generate mice with a conditional deletion of GPR120 in the intestinal epithelium, *Ffar4*$^{flox/flox}$ mice (in which Exon 1 and approx. 1.5 kb of sequence upstream of exon 1 (promoter region) have been flanked by loxP sites) were crossed with *villin-cre* transgenic mice. In the following steps, *VillinCre-Ffar4*$^{flox/+}$ were crossed with *VillinCre-Ffar4*$^{flox/+}$ to obtain *VillinCre-Ffar4*$^{flox/flox}$ mice (named GPR120$^{\Delta IEC}$) and *VillinCre-Ffar4*$^{+/+}$ (named WT) littermates, that were used for the experiments. In these mice, deletion of exon 1 and proximal promoter results in loss of function of the *Ffar4* gene, by preventing transcription of the *Ffar4* mRNA and by deleting the GPR120 transmembrane domains 1 to 4. All mice were maintained in a specific pathogen free (SPF) facility certified by Charles River Laboratories International. Housing was temperature controlled, with a 12 light/12 dark hour cycle. Procedures involving mice conformed to institutional guidelines in agreement with national and international law and obtained ethical approval from the Italian Ministry of Health. The study follows the ARRIVE guidelines for the *in vivo* studies carried out on animals.

Genotyping of mouse tail DNA by PCR: Pups were tailed and toed (for identification) around 3-weeks of age. Transgenic animals (GPR120$^{\Delta IEC}$) were distinguished from heterozygous *VillinCre*-GPR120$^{+/-}$ (Het) and wild-type *VillinCre*-GPR120$^{+/+}$ (WT) littermates by PCR. The DNA was collected from the tail tissue by heating, followed by the addition of 300 µL of neutralization solution (NaOH 60mM, TRIS-HCl 1M pH8). Primers designed to specifically amplify the sequence of interest (see table below), were added with Taq Polymerase and DNA to the master mix, according to manufacturer's instructions, and after the PCR reaction, products were separated on a 2% agarose gel and visualized with Bio-Rad ChemiDoc Imager.

Gene	***Forward primer***	***Reverse primer***
Ffar4	5'GAGCGCATGGTGTGCATCG 3'	3'CACGGCTTTGGTCAGATCC 5'
VillinCre	5'CAAGCCTGGCTCGACGGCC 3'	3' CGCGAACATCTTCAGGTTCT 5'

AOM/DSS-induced colitis-associated colorectal cancer: CAC was induced by a single intraperitoneal injection of azoxymethane (AOM, 10mg/kg, Sigma-Aldrich) in 7 weeks-old C57BL/6 mice and kept on regular water for 7 days. After 7 days, mice were subjected to four oral cycles of 2% of dextran sulfate sodium (DSS) (molecular mass, 40 kDa; MpBio, cat. n°160110) in drinking water for one week followed by one week of normal drinking water. Body weight, stool consistency and rectal bleeding were monitored every two days. The consistency of stool was scored as 0-normal, 1-soft formed, 2- diarrhea-like, 3-watery, 4- not formed and with blood. Presence of blood was detected using Hemoccult kit (Beckman Coulter, cat. n°395034) and scored with increasing numbers starting from 0-no blood to 4- copious and eye-visible amount of blood. Mice were sacrificed after 57 days from the first DSS exposure by CO_2, after endoscopy. Colitis severity was scored using a disease activity index (DAI) score based on daily evaluation of body weight, diarrhea and presence of blood in stools. Scoring of tumor development was evaluated by a high-resolution video miniendoscope (Karl Storz, Tuttlingen, Germany), on the basis of the tumor size and the number of tumors, as described previously[60]. At sacrifice, part of the colon was flash frozen (at -80°C) for mRNA analysis and part was fixed in formalin overnight, included in paraffin and sectioned for histological analysis.

Immunohistochemistry and Immunofluorescence stainings: For immunohistochemistry, three-micrometer formalin-fixed paraffin-embedded colon sections were cut, dewaxed and hydrated. Antigen retrieval was conducted using Citrate buffer 10mM in warm bath for 20 minutes. Endogenous peroxidase was blocked for 15 minutes at room temperature, and then non-specific sites were blocked by Rodent Block (BioCare Medical, cat. n° RBM961G) or Background Sniper (BioCare Medical, cat. n° BS966). Slides were next incubated with the primary antibody against Ki67 [rabbit α-human/mouse (Abcam cat n° ab15580) 1:600 dilution] or ß-catenin [rabbit α-human/mouse (Abcam cat n°ab6302) 1:800 dilution] or GPR120 [rabbit α-human/mouse (Abcam cat n° ab223512) 1:300 dilution] for two hours at room temperature. Subsequently, sections were incubated with the secondary antibody (MACH1 universal HRP-polymer detection, cat. n° M1U539G) at room temperature for 30 min, followed by PBST washing. The immunostaining was visualized with brown DAB (Dako, Carpinteria, CA, USA) and counterstained with Hematoxylin, dehydrated and covered with coverslips.

For immunofluorescence staining, frozen sections were fixed with PFA4% and then permealized using PBS + 0,01% Triton. After incubation with primary α-GPR120, 1:200 dilution; α-Jam A 1:20 dilution; α-Pan Cytokeratin (Abcam cat n° ab86734) 1:100 dilution] and secondary antibodies (1:500 dilution), slides were counterstained with DAPI. Control slides were obtained by omitting the use of primary antibodies.

For the immunofluorescence performed on cells, $6x10^4$ Caco-2 cells were resuspended in 100 µL Matrigel (Corning, cat n° 356255), plated on 8-well chamber slide (ibidi, cat n° 80826) and let to growth for 5 days. When polarization was detectable under microscope, cells were washed with PBS and fixed with 4% PFA for 10 minutes. After washing step with EtOH 70%, cells were permealized with PBS+ 0.02 Tween for 20 minutes, then primary antibodies (α-GPR120, 1:50 dilution; α-Jam A 1:20 dilution) were incubated overnight at 4°C. The day after, cells were washed and incubated with secondary antibodies (1:1000 dilution) for 30 minutes, then counterstained with DAPI. Images were taken with Leica SP8I Confocal Microscopy.

Histological Analysis: Images were acquired using the VS120 DotSlide system (Olympus), and immunostainings were evaluated by ImageJ, using both Olympus and IHC plugins. Olympus plugin allowed to open the file without affecting the resolution of the image; the IHC protocol of ImageJ software automatically detected DAB positive areas; upon conversion of the picture into 8-bit, the brown color was adjusted with threshold and then positive particles were analyzed. For histological analyses, FFPE sections were stained with Hematoxylin and Eosin, according to the standard procedure. The stained sections were scored by an experienced pathologist in a blinded manner.

In vivo quantification of intestinal permeability: Intestinal permeability was evaluated by perfusion of the mouse intestine with the azo Evans Blue dye, as previously described[61]. 8 weeks old mice were anesthetized with a mixture of ketamine and xylazine, the abdomen was opened and a 3 cm proximal portion of the ileum from the ileocecal junction was ligated by silk suture with care to prevent injury to the superior mesenteric vessels. The ileal-luminal contents were washed out gently with 4-5 mL of PBS. The ileo-cecal end was ligated to prepare the ileal loop (3 cm), and then 5ml/mouse at rate of 1ml/minute of Evans blue in PBS was injected into the loop. After 60 min, mice were sacrificed by decapitation and the ileal loop was rapidly dissected out, opened, rinsed with PBS, dried on filter paper at 37 °C for 24 h, and then weighed and incubated with 3 mL of Dymethil Formamide at 50 °C for 24 h. The amount of dye eluted was estimated using a spectrophotometer at a wavelength of 620 nm. The amount of Evans blue permeating into the intestinal wall was calculated based on the standard curve of Evans blue in formamide.

Fluorescence in situ Hybridization: Healthy $GPR120^{\Delta IEC}$ and WT 8 weeks old mice were fed for two weeks with cornmeal mush, then sacrificed by CO_2 and colon tissues included in OCT without any washing steps. Cryosections of 8µm were fixed with Metacarnoy solution (75%MetOH + 25% Acetic Acid) for 4 hours at room temperature, then washed in EtOH and dried in the oven for 30 minutes.

The hybridization area was marked with diamond cutter in order to localize it during the rest of procedure. Each slide was stained with a FISH bacterial probe (Invitrogen) diluted in freshly prepared Hybridization Buffer (NaCl 2M; TRIS HCl 1M; SDS 10%; H_20). The hybridization chamber was prepared and then loaded into DAKO machine overnight. Rubber cement was removed to wash slides in water-bath at 55°C for 20 minutes. Washes in buffer + 2%BSA were performed to remove nonspecific hybrids. Colon sections were incubated with primary [Muc2 (Santa Cruz, B306.1; cat n° sc-59859), mouse α-human/mouse, 1:25 dilution] and secondary (goat α-mouse, 1:1000 dilution) antibodies at room temperature for 1 hour and then stained with DAPI. Images were acquired with an Olympus FV1000/TIRF microscope.

In vitro measurement of epithelial barrier integrity: Transepithelial/transendothelial electrical resistance (TEER) is a quantitative technique that allows to evaluate the epithelial barrier integrity in cell culture models. The setup consists of a cellular monolayer cultured on semipermeable filter which defines the apical portion from the basolateral one. It is composed by two electrodes: one is placed in the upper compartment and the other in the lower, separated by the cellular monolayer. The ohmic resistance determined by applying a direct current (DC) voltage to the electrodes gives an estimation of the cellular monolayer permeability. The higher the resistance, the lower the permeability[62]. This system has been used on monolayers of Caco-2 and LoVo cells, in which cells of our interest were plated in the lower compartment at ~60% of confluency, treated with siRNA and, 48hours post-transfection, the measurement was performed.

Collection of mucus layer, protein gels and liquid chromatography in tandem mass spectrometry (LC-MS/MS): Healthy GPR120$^{\Delta IEC}$ and WT 8 weeks old mice were sacrificed and colon was gently washed with PBS. The colon was opened longitudinally and mucus was scraped off the epithelial layer and collected by pipette. Collected mucus were mixed with protease inhibitors (PI 50x; PMSF 100x; NaVPO 200x) and then stored at -20°C until use. Two-dimensional electrophoresis procedure is schematized in **Supplementary Figure 6**.

2-DE: About 250 µg of extracted proteins were dissolved in 125µL of rehydration buffer (8M urea, 4% CHAPS (w/v), 65 mM DTE, 0,8% carrier ampholytes (v/v), 0,5% bromophenol blue) and loaded onto 7 cm IPG strips, with nonlinear (NL) pH 3-10 or linear pH 4-7 gradient range (GE Healthcare, UK). Strips were rehydrated without applying voltage for 1h at 20°C. The first dimensional IEF was carried out at 15°C using an Ettan IPGphor 3 system (GE Healthcare, UK). Three hours later, the IEF run was stopped to allow positioning of small pieces of paper between the IPG strip and electrodes. Reduction and alkylation steps were performed between the first and the second dimension. The

focused IPG strips were incubated for 15 min at room temperature in 6M urea, 2% (w/v) SDS, 50 mM Tris pH 6.8, glycerol 30%, containing 2% (w/v) DTE, followed by a second incubation of 15 min in the same buffer containing 2,5% (w/v) iodoacetamide and 0,5% bromophenol blue. At the end of the IEF step, strips were hold in place with 0,4% low melting temperature agarose and loaded onto 8 x 6 cm slabs, 12,5% SDS polyacrylamide gels. Electrophoresis was carried out at a constant current of 10 mA per gel in a PROTEAN II xi 2-D BioRad Cell equipment (Berkeley, California), until the buffer front line was 1 mm from the bottom of the gel.

LC- MS/MS: Identification of the protein(s) under the spots was carried out on an LC-MS/MS (Thermo Finnigan, USA) system consisting of a thermostated column oven Surveyor autosampler controlled at 25°C, a quaternary gradient surveyor MS pump equipped with a diode array detector, and a Linear Trap Quadrupole (LTQ) mass spectrometer with electrospray ionization ion source controlled by Xcalibur software 1.4. Analytes were separated by RP-HPLC on a Jupiter (Phenomenex, USA) C18 column (150x2 mm, 4 µm, 9 Å particle size) using a linear gradient (2-16% solvent B in 60 min) in which solvent A consisted of 0.1% aqueous formic acid (FA) and solvent B consisted of Acetonitrile (ACN) containing 0.1% FA. Flow-rate was 0,2 mL/min. Mass spectra were generated in positive ion mode under constant instrumental conditions: source voltage 5.0 kV, capillary voltage 46 V, sheath gas flow 40 (arbitrary units), auxiliary gas flow 10 (arbitrary units), sweep gas flow 1 (arbitrary units), capillary temperature 200 °C, tube lens voltage -105 V. MS/MS spectra, obtained by CID studies in the linear ion trap, were performed with an isolation width of 3 Th m/z, the activation amplitude was 35% of ejection RF amplitude that corresponds to 1.58 V. Data processing was performed using Peaks studio software.

Western Blot: Samples obtained from the two-dimensional electrophoresis protocol were lysed in RIPA buffer, followed by protein quantification. Upon separation on electrophoresis gel, proteins were transferred onto a nitrocellulose membrane by using a Trans-Blot® Turbo™ Transfer System (BioRad). B- actin was used as loading control. Nonspecific binding was blocked with Tris-buffered saline (TBS) containing 1% non-fat dried milk for 1 hour, followed by overnight incubation at 4°C with the mouse anti-human MUC2 antibody, that recognizes also the mouse protein. Membranes were washed and then incubated for 2 hours at room temperature with the appropriate HRP-conjugated secondary antibody (1:3000; GE Healthcare). Membranes were then incubated with Immobilon Western Chemilum (Millipore) and bands were detected by Chemidoc (Bio-Rad Laboratories), using Quantity One software.

Microbiomic analysis: Stool samples were collected from healthy mice and immediately frozen at -80°C. Metagenomic DNA was extracted from about 50 mg of feces using PowerSoil DNA isolation Kit (MO Bio Laboratories) according to manufacturer's instructions. Subsequently, the bacterial community structure was profiled by 16S rRNA gene profiling. In brief, Pro-bio_Uni and Probio_Rev primers were used to amplify a partial region of the 16S rRNA encompassing the V3 variable region, then amplicons were sequenced using Illumina MiSeq System.

Analysis of Short Chain Fatty Acids and Lipid Mediators: Stool samples from healthy (n=10) and AOM/DSS treated mice (n=4) were collected and immediately frozen at -80°C until use. SCFAs were quantified following the protocol published by Hoving et al[63]. Briefly, aqueous feces extract was prepared, a mix of isotopically labelled internal standards (containing acetic acid-d4, propionic acid-d6 and butyric acid-d8) was added and analytes were derivatized using Pentafluorobenzyl Bromide. The analytes of interest were extracted in *n*-hexane and measured by GC-MS. Analytes were chemically ionized (CI) and the MS was operated in negative mode using a single ion monitoring (SIM) method.

From the same samples, lipid mediators were analyzed. Briefly, 20 µL aqueous feces extract was mixed with 60 µL MetOH and 3.2 µL of a mix of isotopically labelled internal standards (containing 50 ng/mL Prostaglandin E_2-d4, Leukotriene B_4-d4 and 15-HETE-d8 and 500 ng/mL DHA-d5) in MetOH. The sample was mixed, incubated at -20 °C for 20 min. and centrifuged (16.1 krcf, 10 min., 4 °C). 50 µL supernatant was diluted with 50 µL water, vortexed and measured by LC- MS/MS as described elsewhere[64].

In vitro cell proliferation, and siRNA transfection: Human colorectal cancer cell lines [Caco-2 (ATTC HTB-37), and LoVo (ATCC CCL-229)] were maintained in culture with DMEM medium (Merck, cat no SLM-241-B) containing 10% (v/v) Fetal Bovine Serum (FBS) and 1% antibiotics (Penicillin-Streptomycin), at 37°C and 5% CO_2.

For proliferation assays, cells were seeded in 6-well plates at 100.000 cells/well (~ 40% confluency), in complete medium and transfected with siRNA against the free fatty acid receptor 4 (*FFAR4*) or control scramble siRNA, by using Lipofectamine 2000 (Invitrogen, cat. n° 11668019), following manufacturer's instructions. siRNA oligos and their scramble siRNA control were designed by using the siRNA Wizard Software 3.1 and are reported in **Table 1**.

Briefly, 2500 ng/µl of siRNA oligomers was diluted in 50µl Gibco™ OptiMEM™ I Reduced Serum DMEM medium and 1µl of Lipofectamine 2000 were diluted in the same amount of Gibco™ OptiMEM™ I Reduced Serum (amounts and volumes are given on a per well basis). After 5-minute

incubation, the diluted oligomers and the diluted Lipofectamine 2000 were combined and incubated for 20 minutes at room temperature. The oligomer-Lipofectamine 2000 complexes were then added to each well of 6-wells cell culture plates and incubated for 48 hours at 37°C in CO_2 incubator. After two days, cells were trypsinized by Trypsin- EDTA and counted using a Burker chamber. Cells from each experimental group were used to extract total RNA, as described above.

qRT-PCR: Total RNA was extracted from colon tissues and cancer cell lines using RNeasy Mini Kit (Qiagen, cat. no 74104), according to the manufacturer's instructions. RT-PCR was performed using Fast SYBR Green Master Mix (Applied Biosystem, cat. n°1408115) and Viia7 Detection system (Applied Biosystem). Glyceraldehyde 3-phosphate dehydrogenase (GAPDH) gene was used as internal control. Relative gene expression was determined by the $2^{-\Delta Ct}$ method. The specific oligonucleotide primers used are listed in **Table 2**.

Cell cycle analysis and apoptosis by FACS: For cell cycle analysis, scramble siRNA-, and siRNA-transfected cells were washed with PBS and incubated in EtOH 80% for 30 minutes. After centrifugation and washing steps, cells were resuspended in DAPI/TX-100 solution (9mL PBS; 1mL Triton X-100; 10µL DAPI 1µg/mL) and incubated for 30 minutes at room temperature. Cell cycle analysis was next performed by FlowJo v.10.6.1 software, which provides a simple interface to perform sophisticated univariate DNA/Cell Cycle analysis using the Dean-Jett-Fox model[65].
Quantification of apoptotic cells was performed using the Annexin V-FITC Kit (Abcam, cat n° ab14082) and 7-AAD (cat n° 559925), for the exclusion of nonviable cells and detectable in far red, following the manufacturer's instructions. Briefly, $1x10^5$ cells were incubated with 5 microliters of both Annexin V and 7-AAD in the proper buffer for 5 minutes in the dark and then acquired by FACS and analyzed by using FlowJo v.10.6.1.

Isolation of epithelial cells from mouse colon: Colon tissues were collected from healthy wild-type and transgenic 8 weeks old mice and flushed with ice-cold PBS. Tissue was cut in small pieces and washed several times by inverting the 15-ml conical tube. After dissociation in 0,5M EDTA for 30 minutes on an orbital shaker, the tube was shaken for 5 minutes by hand to dissociate epithelium from the basement membrane. The solution was filtered through a 100µm filter to remove the villus fraction. After two centrifugations of 10 minutes at 150g, 4°C, the resulting pellet containing epithelial cells was stored at -80°C until use. Total RNA was extracted as described above and used for RNA-seq.

Human samples: Frozen tissue biopsies of 9 normal tissues, 9 adenomas, and 17 primary adenocarcinomas were obtained from fresh tissue biobank collection at Humanitas Clinical and Research Center, and proceeded for the mRNA extraction. Healthy tissue was collected at a distance of at least 10 cm from tumor lesion. No patient had received any therapy before surgery.

Bioinformatic Analysis: To analyze the differential gene expression of *FFAR4* in normal and cancer tissues, we took advantage of the GENT 2 database (http://gent2.appex.kr/gent2/). This database compares *FFAR4* gene expression in various tissues but also its expression across cancer subtypes [like AJJC staging based on the extent of the tumor (T), the extent of spread to the lymph nodes (N), and the presence of metastasis (M)].
For the proteomic analysis, differentially enriched proteins were identified DAVE score +2/-2.
For the microbiomic analysis, the resulting sequence reads were managed by means of the bioinformatic pipeline Quantitative Insights Into Microbial Ecology (QIIME) version 1.7.0[66] with the GreenGenes database (version 13.5), which allowed clustering of sequences into operational taxonomic units (OTUs).

Statistical Analysis: All statistical analyses were performed using Prism GraphPad Prism 8.0 and STATA16 software. Data are presented as the median ± 95% CI (confidence interval). Student *t*-test was used to examine differences between groups with normal distribution, and its non-parametric counterpart (Mann Whitney test) was used if assumptions were not satisfied. A p.value <0,05 was considered statistically significant. The differences in the microbiota composition between wild type and mutant mice were inferred at the OTU level using a Wald test following read count normalization with the DESeq2 negative binomial distribution method.

Table 1: siRNAs sequences

Sample	***Sequence***
siRNA #1	5' GAGTGGCGTAAGCCGACTATT 3'
siRNA #2	5' GTGGCGTAAGCCGACTATTGA 3'
siRNA #3	5' GGCCTGGAGATGCACATTGTT 3'
Scramble	5' GAAGGACGCTGACGTTGATCT 3

603 **Table 2***:* Primer sequences

Gene name	Forward primer	Reverse primer
Ffar 4	5'ATTTTACAGATCACAAAGGCATC 3'	5'AGGCTTACCGTGAGCCTCTTC 3'
Muc 2	5'AGGGCTCGGAACTCCAGAAA 3'	5'CCAGGGAATCGGTAGACATCG 3'
Il1b	5'GAAATGCCACCTTTTGACAGTG 3'	5'TGGATGCTCTCATCAGGACAG 3'
Il6	5'CTGCAAGAGACTTCCATCCAG 3'	5'AGTGGTATAGACAGGTCTGTTGG 3'
Tnfa	5'CAGGCGGTGCCTATGTCTC 3'	5'CGATCACCCCGAAGTTCAGTAG 3'
Gapdh	5'AGGTCGGTGTGAACGGATTTG 3'	5'GGGGTCGTTGATGGCAACA 3'
FFAR4	5'AGACCTCGGAACACCTCCTG 3'	5'AGGCTTACCGTGAGCCTCTTC 3'
CTNNB1	5'CATCTACACAGTTTGATGCTGCT 3'	5'GCAGTTTTGTCAGTTCAGGGA 3'
GAPDH	5'GGAGCGAGATCCCTCCAAAAT 3'	5'GGCTGTTGTCATACTTCTCATGG 3'

604

605

606 **Figure Legends**

607 **Figure 1: GPR120 expression in intestinal epithelial cells. (a**) Representative immunofluorescence
608 images from the human (**upper panel**) and mouse (**lower panel**) frozen colon sections stained with
609 antibodies against GPR120, cytokeratins (Pan CK) and junctional adhesion molecule A (Jam A).
610 Magnification: 20X. Scale bar: 20 μm. (**b**) Representative immunofluorescence images from Caco-2
611 cells, grown in Matrigel as spheroids, stained with antibodies against GPR120 and Jam A highlighting
612 the apical localization of the receptor. Magnification 40x. Scale bar: 50 μm. (**c**) Representative
613 immunofluorescence images from frozen colon tissues of wild-type (WT) and transgenic
614 (GPR120$^{\Delta IEC}$) mice stained with antibodies against GPR120 and Jam A. Magnification: 20x. Scale
615 bar: 50 μm. (**d)** Intestinal permeability was evaluated in healthy GPR120 $^{\Delta IEC}$ mice (n=4) and WT
616 (n=4) by perfusion in the mouse intestine with Evans Blue dye for 60 min. The amount of dye eluted
617 was quantified using a spectrophotometer at a wavelength of 620 nm and results are expressed as OD
618 per gram of colon tissue. (**e**) Frozen colon sections from healthy GPR120 $^{\Delta IEC}$ mice (n=3) and WT
619 (n=3) littermates were stained with FISH using a bacterial probe (red) and an anti-Muc2 antibody
620 (green). The inner mucus layer is indicated with white dashed line. Magnification 40x. Scale bar: 50
621 μm. (**f-g**) TEER was measured in siRNA-treated Caco-2 and LoVo cells and compared with scramble
622 siRNA controls**.** Values are expressed as median ± 95% CI. *p value < 0,05; **p.value < 0,001 by
623 Mann Whitney test.

624

625 **Figure 2: GPR120 expression preserves inner mucus layer integrity. (a)** The expression levels of
626 *Muc2* gene was quantified by qRT-PCR in healthy GPR120$^{\Delta IEC}$(n=3) and WT (n=3) mice. (**b**)
627 Representative bands of Muc2 obtained by western blot on GPR120$^{\Delta IEC}$ and WT mucus samples. (**c)**
628 Mucus layer samples from healthy GPR120$^{\Delta IEC}$ (n=3) and WT (n=3) mice were scraped off the colon
629 and subjected to two-dimensional electrophoresis. Gels from transgenic and WT mucus were
630 overlapped in a high master gel (HMG) by software to identify proteins differentially expressed in
631 the two groups. Red spots belong to WT samples, blue spots belong to GPR120$^{\Delta IEC}$ samples, and
632 green spots are in common between two groups. (**d)** Scatter plot showing all proteins detected by
633 mass-spectrometry and differentially expressed (in red) between GPR120$^{\Delta IEC}$(TG) and WT mice,

according to DAVE score +2/-2. Among dysregulated proteins, Muc2 was significantly downregulated in GPR120$^{\Delta IEC}$ mucus samples. (**e**) A metagenomic analysis was performed on fecal samples of healthy WT (n=5) and GPR120 $^{\Delta IEC}$ (n=6) mice. Plot showing alpha diversity (Shannon index) for microbial communities in the two groups, upon16S rRNA gene sequencing analysis. (**f)** Principal component analysis (PCA) plots showing Weighted (**right panel**) and Unweighted (**left panel**) beta diversity in fecal samples from the two groups. (**g)** DESeq2 analysis showing operational taxonomical units (OTUs) in GPR120 $^{\Delta IEC}$ versus WT fecal samples. Each spot represents a taxonomical unit; red spots represent taxonomical units with statistically significant differences between the two groups. (**h**) OTUs distinguishing WT and GPR120 $^{\Delta IEC}$ mice determined using the DESeq2 negative binomial distribution method on the 16S rRNA gene profiling data of fecal samples. The taxonomic lineage of each taxon is shown: p, phylum; c, class; o, order; f, family; g, genus; s, species. The black-yellow heatmap represents the mean normalized relative abundances of the reported OTUs. Positive fold changes (shown on a red background) designate OTU overrepresentation in GPR120 $^{\Delta IEC}$ mice (KO); negative fold changes (shown on a blue background) designate the OTU overrepresentation in WT mice. padj, adjusted p values were represented in a heatmap. (**i**) Bar plots showing quantification of SCFAs, including acetate, butyrate, propionate and valerate in fecal samples of healthy GPR120$^{\Delta IEC}$ (n=10) and WT (n=9) littermates. Values are expressed as median ± 95% CI. *p.value<0,05 by Mann Whitney test.

Figure 3: Conditional deletion of GPR120 in the intestinal epithelium affects colitis-associated cancer development. (**a**) GPR120$^{\Delta IEC}$ (n=7) and WT (n=7) mice were subjected to the AOM/DSS-induced model of CRC as schematize. (**b**) Representative endoscopic images showing mouse polyps at day 57. Tumor density (**c**) and size (**d**) assessed at day 57 by endoscopic scoring. The size depends upon the average of diameter: size 1 very small but detectable tumor, size 2 tumor covering up to one-eighth of colonic circumference, size 3 tumor covering up to one-fourth of the colonic circumference, size 4 tumor covering up to half of the colonic circumference, and size 5 tumor covering more than half of the colonic circumference. (**e, f**) Representative paraffin-embedded colon sections from tumor bearing GPR120$^{\Delta IEC}$ (n=7) and WT (n=7) mice stained for Ki67 (**e**) and relative quantification expressed as percentage of immune positive area (**f**). Magnification 20x. Scale bar: 100 μm. (**g**) Histological score quantifying Low grade (**left panel**), High grade (**central panel**) adenomas, and adenocarcinoma (**right panel**) on paraffin-embedded colon sections (n=7 per group) stained with Hematoxylin & Eosin (H&E).

Figure 4: **Loss of epithelial GPR120 correlates with CRC development** (**a**) The expression levels of *FFAR4* gene were quantified by qRT-PCR in healthy colon (n=9), adenomas (n=9) and adenocarcinoma (n=17) from human samples. (**b**) Representative immunostaining for GPR120 in human samples of Normal mucosa (n=6), High-Grade Adenomas (HGA) (n=6), T1 (n=6) and T2 (n=6) tumors, (**c**) and relative quantification of positive area. Values are expressed as median percentage of positive over total area ± 95% CI. Magnification: 20X. Scale bar: 50 μm. (**d**) Gene expression of *FFAR4* in the indicated tissues annotated in the GENT2 database, expressed as Log2 and plotted according to tissue type. Green box represents *FFAR4* expression in CRC and healthy colon tissue. Values are expressed as median ± 95% CI. *p value < 0,05; **p.value < 0,001 by Mann Whitney test.

Figure 5: GPR 120 protein induces Wnt/β-catenin signaling. (a) Caco-2 (**left panel**) and LoVo (**right panel**) cells were transfected with siRNA against *FFAR4* and scramble siRNA controls, after 48 hours from transfection proliferation was assessed by using the Burker chamber and expressed as absolute cell number. (**b**) The cell cycle distribution of siRNA-treated Caco-2 and LoVo cells was performed by FACS 48 hours after siRNA transfection, and upon DAPI staining. Quantifications of Caco-2 and LoVo cells labeled with DAPI in each phase of the cell cycle are shown. Values are median ± 95% CI of biological triplicates. (**c**) Quantification of *CCND1* gene transcripts by qRT-

PCR in Caco-2 and LoVo cells treated with either siRNA against *FFAR4* or scramble siRNA. (**d**) Intracellular calcium was measured 48hours after siRNA transfection, by using a colorimetric kit and results are expressed as mM of calcium concentration. Biological triplicates. (**e**) The expression of β-catenin gene transcript (*Ctnnb1*) was extrapolated from our RNA-seq analysis performed on the epithelium of healthy GPR120 $^{\Delta IEC}$ (n=3) and WT (n=3) mice, and expressed as log2 RPKM. (**f**) *Ctnnb1*expression levels were quantified by qRT-PCR in AOM/DSS-induced GPR120 $^{\Delta IEC}$ (n=7) and WT (n=7) mice. (**g, h**) Paraffin-embedded colon sections from GPR120 $^{\Delta IEC}$ (n=7) and WT (n=7) mice were immunostained using an anti-β-catenin antibody. Magnification: 20X. Scale bar: 100 μm. Representative immunostainings are shown in (**g**), with relative quantification of immune-positive areas in (**h**). Values are expressed as median percentage of positive over total area ± 95% CI. (**i**) Quantification of *CTNNB1* gene transcripts by qRT-PCR in Caco-2 and LoVo cells treated with either siRNA against *FFAR4* or scramble siRNA. Values are expressed as median ± 95% CI of biological triplicates. *p.value < 0,05; **p.value < 0,001; ****p.value < 0,00005 by Mann Whitney test.

Figure 6: **The loss of epithelial GPR120 impacts on fecal lipids metabolites**. (**a,b**) ω-3 PUFAs (**a**) and DHA-derived metabolites (**b**) were quantified through LC-MS/MS analysis and expressed as area ratio/feces concentration. Values are expressed as median ± 95% CI. *p.value < 0,05; **p.value < 0,001; ****p.value < 0,00005 by Mann Whitney test.

Acknowledgement

We want to thank Michela Lizier for mouse generation.

Author contribution

Study concept and design: FR, SV, LL, SD. Acquisition of data: FR, SS. Analysis and interpretation of data: FR, SV, LL. Drafting manuscript: FR. Critical revision of the manuscript for important intellectual content: SV, LL, PI, MG, SG, AM. Statistical analysis: FR. Administrative, technical or material support: VG, VG, MC, MH, SG, VA, LM. Study supervision: SV, SD.

All the Authors read and approved the final manuscript. No conflicts of interest exist.

References

1. Morris, A. J. & Malbon, C. C. Physiological regulation of G protein-linked signaling. *Physiological Reviews* **79**, 1373–1430 (1999).
2. Bar-Shavit, R. *et al.* G protein-coupled receptors in cancer. *International Journal of Molecular Sciences* **17**, (2016).
3. Feigin, M. E. Harnessing the genome for characterization of G-protein coupled receptors in cancer pathogenesis. *FEBS Journal* **280**, 4729–4738 (2013).
4. Mobraten, K., Haug, T. M., Kleiveland, C. R. & Lea, T. Omega-3 and omega-6 PUFAs induce the same GPR120-mediated signalling events, but with different kinetics and intensity in Caco-2 cells. *Lipids Health Dis.* **12**, (2013).

5. Talukdar, S., Olefsky, J. M. & Osborn, O. Targeting GPR120 and other fatty acid-sensing GPCRs ameliorates insulin resistance and inflammatory diseases. *Trends in Pharmacological Sciences* **32**, 543–550 (2011).
6. Anbazhagan, A. N. *et al.* A novel anti-inflammatory role of GPR120 in intestinal epithelial cells. *Am. J. Physiol. - Cell Physiol.* **310**, C612–C621 (2016).
7. Chinthakunta, N., Cheemanapalli, S., Chinthakunta, S., Anuradha, C. M. & Chitta, S. K. A new insight into identification of in silico analysis of natural compounds targeting GPR120. *Netw. Model. Anal. Heal. Informatics Bioinforma.* **7**, (2018).
8. Marion-Letellier, R., Savoye, G. & Ghosh, S. Polyunsaturated fatty acids and inflammation. *IUBMB Life* **67**, 659–667 (2015).
9. Wang, X. *et al.* Fatty acid receptor GPR120 promotes breast cancer chemoresistance by upregulating ABC transporters expression and fatty acid synthesis. *EBioMedicine* **40**, 251–262 (2019).
10. Zhang, M. & Qiu, S. Activation of GPR120 promotes the metastasis of breast cancer through the PI3K/Akt/NF-κB signaling pathway. *Anticancer. Drugs* **30**, 260–270 (2019).
11. Cui, Z. *et al.* G-protein-coupled receptor 120 regulates the development and progression of human esophageal cancer. *Oncol. Rep.* **40**, 1147–1155 (2018).
12. Liu, Z. *et al.* Omega-3 fatty acids and other FFA4 agonists inhibit growth factor signaling in human prostate cancer cells. *J. Pharmacol. Exp. Ther.* **352**, 380–394 (2015).
13. Fukushima, K. *et al.* Different roles of GPR120 and GPR40 in the acquisition of malignant properties in pancreatic cancer cells. *Biochem. Biophys. Res. Commun.* **465**, 512–515 (2015).
14. Wu, Q. *et al.* Identification of G-protein-coupled receptor 120 as a tumor-promoting receptor that induces angiogenesis and migration in human colorectal carcinoma. *Oncogene* **32**, 5541–5550 (2013).
15. Senatorov, I. S. & Moniri, N. H. The role of free-fatty acid receptor-4 (FFA4) in human cancers and cancer cell lines. *Biochemical Pharmacology* **150**, 170–180 (2018).
16. Thoo, L., Noti, M. & Krebs, P. Keep calm: the intestinal barrier at the interface of peace and war. *Cell Death and Disease* **10**, (2019).
17. Srikanth, C. V. & McCormick, B. A. Interactions of the Intestinal Epithelium with the Pathogen and the Indigenous Microbiota: A Three-Way Crosstalk. *Interdiscip. Perspect. Infect. Dis.* **2008**, 1–14 (2008).
18. Jobin, C. Colorectal cancer: CRC - All about microbial products and barrier function? *Nat. Rev. Gastroenterol. Hepatol.* **9**, 694–696 (2012).
19. Kang, H. *et al.* Loss of E-cadherin and MUC2 expressions correlated with poor survival in

patients with stages II and III colorectal carcinoma. *Ann. Surg. Oncol.* **18**, 711–719 (2011).

20. Niv, Y. & Rokkas, T. Mucin Expression in Colorectal Cancer (CRC): Systematic Review and Meta-Analysis. *Journal of Clinical Gastroenterology* **53**, 434–440 (2019).
21. Paulsen, S. J. *et al.* Expression of the fatty acid receptor GPR120 in the gut of diet-induced-obese rats and its role in GLP-1 secretion. *PLoS One* **9**, (2014).
22. El Marjou, F. *et al.* Tissue-specific and inducible Cre-mediated recombination in the gut epithelium. *Genesis* **39**, 186–193 (2004).
23. Vetrano, S. *et al.* Unique Role of Junctional Adhesion Molecule-A in Maintaining Mucosal Homeostasis in Inflammatory Bowel Disease. *Gastroenterology* **135**, 173–184 (2008).
24. Petti, L. *et al.* Unveiling role of sphingosine-1-phosphate receptor 2 as a brake of epithelial stem cell proliferation and a tumor suppressor in colorectal cancer. *J. Exp. Clin. Cancer Res.* **39**, (2020).
25. Milligan, G., Alvarez-Curto, E., Hudson, B. D., Prihandoko, R. & Tobin, A. B. FFA4/GPR120: Pharmacology and Therapeutic Opportunities. *Trends in Pharmacological Sciences* **38**, 809–821 (2017).
26. Apáti, Á., Jánossy, J., Brózik, A., Bauer, P. I. & Magócsi, M. Calcium induces cell survival and proliferation through the activation of the MAPK pathway in a human hormone-dependent leukemia cell line, TF-1. *J. Biol. Chem.* **278**, 9235–9243 (2003).
27. Olmeda, D., Castel, S., Vilaró, S. & Cano, A. β-catenin regulation during the cell cycle: Implications in G2/M and apoptosis. *Mol. Biol. Cell* **14**, 2844–2860 (2003).
28. Campieri, M. & Gionchetti, P. Bacteria as the cause of ulcerative colitis. *Gut* **48**, 132–135 (2001).
29. Elinav, E. *et al.* Inflammation-induced cancer: Crosstalk between tumours, immune cells and microorganisms. *Nature Reviews Cancer* **13**, 759–771 (2013).
30. Rodríguez-Piñeiro, A. M. *et al.* Studies of mucus in mouse stomach, small intestine, and colon. II. Gastrointestinal mucus proteome reveals Muc2 and Muc5ac accompanied by a set of core proteins. *Am. J. Physiol. - Gastrointest. Liver Physiol.* **305**, (2013).
31. Bäckhed, F., Ley, R. E., Sonnenburg, J. L., Peterson, D. A. & Gordon, J. I. Host-bacterial mutualism in the human intestine. *Science* **307**, 1915–1920 (2005).
32. Johansson, M. E. V., Thomsson, K. A. & Hansson, G. C. Proteomic analyses of the two mucus layers of the colon barrier reveal that their main component, the Muc2 mucin, is strongly bound to the fcgbp protein. *J. Proteome Res.* **8**, 3549–3557 (2009).
33. Velcich, A. *et al.* Colorectal cancer in mice genetically deficient in the mucin Muc2. *Science (80-.).* **295**, 1726–1729 (2002).

794 34. Hsu, H. P. *et al.* Mucin 2 silencing promotes colon cancer metastasis through interleukin-6
795 signaling. *Sci. Rep.* **7**, (2017).
796 35. Naydenov, N. G. *et al.* Nonmuscle myosin IIA regulates intestinal epithelial barrier in vivo
797 and plays a protective role during experimental colitis. *Sci. Rep.* **6**, (2016).
798 36. Wallace, K. N. *et al.* Mutation of smooth muscle myosin causes epithelial invasion and cystic
799 expansion of the zebrafish intestine. *Dev. Cell* **8**, 717–726 (2005).
800 37. Maddugoda, M. P., Crampton, M. S., Shewan, A. M. & Yap, A. S. Myosin VI and vinculin
801 cooperate during the morphogenesis of cadherin cell-cell contacts in mammalian epithelial
802 cells. *J. Cell Biol.* **178**, 529–540 (2007).
803 38. Peng, X., Nelson, E. S., Maiers, J. L. & DeMali, K. A. New Insights into Vinculin Function
804 and Regulation. in *International Review of Cell and Molecular Biology* **287**, 191–231
805 (Elsevier Inc., 2011).
806 39. Feng, W., Ao, H. & Peng, C. Gut microbiota, short-chain fatty acids, and herbal medicines.
807 *Frontiers in Pharmacology* (2018). doi:10.3389/fphar.2018.01354
808 40. Yu, Y.-N. & Fang, J.-Y. Gut Microbiota and Colorectal Cancer. *Gastrointest. tumors* **2**, 26–
809 32 (2015).
810 41. Venegas, D. P. *et al.* Short chain fatty acids (SCFAs)mediated gut epithelial and immune
811 regulation and its relevance for inflammatory bowel diseases. *Frontiers in Immunology* **10**,
812 (2019).
813 42. Sengupta, S., Muir, J. G. & Gibson, P. R. Does butyrate protect from colorectal cancer?
814 *Journal of Gastroenterology and Hepatology (Australia)* **21**, 209–218 (2006).
815 43. Tjalsma, H., Boleij, A., Marchesi, J. R. & Dutilh, B. E. A bacterial driver-passenger model
816 for colorectal cancer: Beyond the usual suspects. *Nature Reviews Microbiology* (2012).
817 doi:10.1038/nrmicro2819
818 44. Gagnière, J. *et al.* Gut microbiota imbalance and colorectal cancer. *World Journal of*
819 *Gastroenterology* (2016). doi:10.3748/wjg.v22.i2.501
820 45. Everard, A. *et al.* Cross-talk between Akkermansia muciniphila and intestinal epithelium
821 controls diet-induced obesity. *Proc. Natl. Acad. Sci. U. S. A.* (2013).
822 doi:10.1073/pnas.1219451110
823 46. Everard, A. *et al.* Cross-talk between Akkermansia muciniphila and intestinal epithelium
824 controls diet-induced obesity. *Proc. Natl. Acad. Sci. U. S. A.* **110**, 9066–9071 (2013).
825 47. Zhang, K. *et al.* G-protein-coupled receptors mediate ω-3 PUFAs-inhibited colorectal cancer
826 by activating the Hippo pathway. *Oncotarget* **7**, 58315–58330 (2016).
827 48. Novellasdemunt, L., Antas, P. & Li, V. S. W. Targeting Wnt signaling in colorectal cancer.

A review in the theme: Cell signaling: Proteins, pathways and mechanisms. *Am. J. Physiol. - Cell Physiol.* **309**, C511–C521 (2015).

49. Kobayashi, M. *et al.* Nuclear translocation of beta-catenin in colorectal cancer. *Br. J. Cancer* **82**, 1689–1693 (2000).

50. Xing Pei Hao, Pretlow, T. G., Rao, J. S. & Pretlow, T. P. β-catenin expression is altered in human colonic aberrant crypt foci. *Cancer Res.* (2001).

51. Brabletz, T. *et al.* Variable β-catenin expression in colorectal cancers indicates tumor progression driven by the tumor environment. *Proc. Natl. Acad. Sci. U. S. A.* **98**, 10356–10361 (2001).

52. Norat, T. *et al.* Meat, fish, and colorectal cancer risk: The European prospective investigation into cancer and nutrition. *J. Natl. Cancer Inst.* **97**, 906–916 (2005).

53. Hall, M. N., Chavarro, J. E., Lee, I. M., Willett, W. C. & Ma, J. A 22-year prospective study of fish, n-3 fatty acid intake, and colorectal cancer risk in men. *Cancer Epidemiol. Biomarkers Prev.* **17**, 1136–1143 (2008).

54. Aglago, E. K. *et al.* Consumption of Fish and Long-chain n-3 Polyunsaturated Fatty Acids Is Associated With Reduced Risk of Colorectal Cancer in a Large European Cohort. *Clin. Gastroenterol. Hepatol.* **18**, 654-666.e6 (2020).

55. Tutino, V. *et al.* Elevated aa/epa ratio represents an inflammatory biomarker in tumor tissue of metastatic colorectal cancer patients. *Int. J. Mol. Sci.* **20**, (2019).

56. Mika, A. *et al.* Preferential uptake of polyunsaturated fatty acids by colorectal cancer cells. *Sci. Rep.* **10**, (2020).

57. Zhao, J., Wang, H., Shi, P., Wang, W. & Sun, Y. GPR120, a potential therapeutic target for experimental colitis in IL-10 deficient mice. *Oncotarget* **8**, 8397–8405 (2017).

58. Rosella, O., Sinclair, A. & Gibson, P. R. Polyunsaturated fatty acids reduce non-receptor-mediated transcellular permeation of protein across a model of intestinal epithelium in vitro. *J. Gastroenterol. Hepatol.* **15**, 626–631 (2000).

59. Anti, M. *et al.* Effect of ω-3 fatty acids on rectal mucosal cell proliferation in subjects at risk for colon cancer. *Gastroenterology* **103**, 883–891 (1992).

60. Becker, C., Fantini, M. C. & Neurath, M. F. High resolution colonoscopy in live mice. *Nat. Protoc.* **1**, 2900–2904 (2007).

61. Lange, S., Delbro, D. S. & Jennische, E. Evans blue permeation of intestinal mucosa in the rat. *Scand. J. Gastroenterol.* **29**, 38–46 (1994).

62. Srinivasan, B. *et al.* TEER Measurement Techniques for In Vitro Barrier Model Systems. *Journal of Laboratory Automation* **20**, 107–126 (2015).

63. Hoving, L. R., Heijink, M., van Harmelen, V., van Dijk, K. W. & Giera, M. GC-MS analysis of short-chain fatty acids in feces, cecum content, and blood samples. in *Methods in Molecular Biology* **1730**, 247–256 (Humana Press Inc., 2018).
64. Körner, A. *et al.* Inhibition of Δ24-dehydrocholesterol reductase activates pro-resolving lipid mediator biosynthesis and inflammation resolution. *Proc. Natl. Acad. Sci. U. S. A.* **116**, 20623–20634 (2019).
65. Dean, P. N. & Jett, J. H. Mathematical analysis of dna distributions derived from flow microfluorometry. *J. Cell Biol.* **60**, 528–527 (1974).
66. Caporaso, J. G. *et al.* QIIME allows analysis of high-throughput community sequencing data. *Nature Methods* **7**, 335–336 (2010).

.

Figures

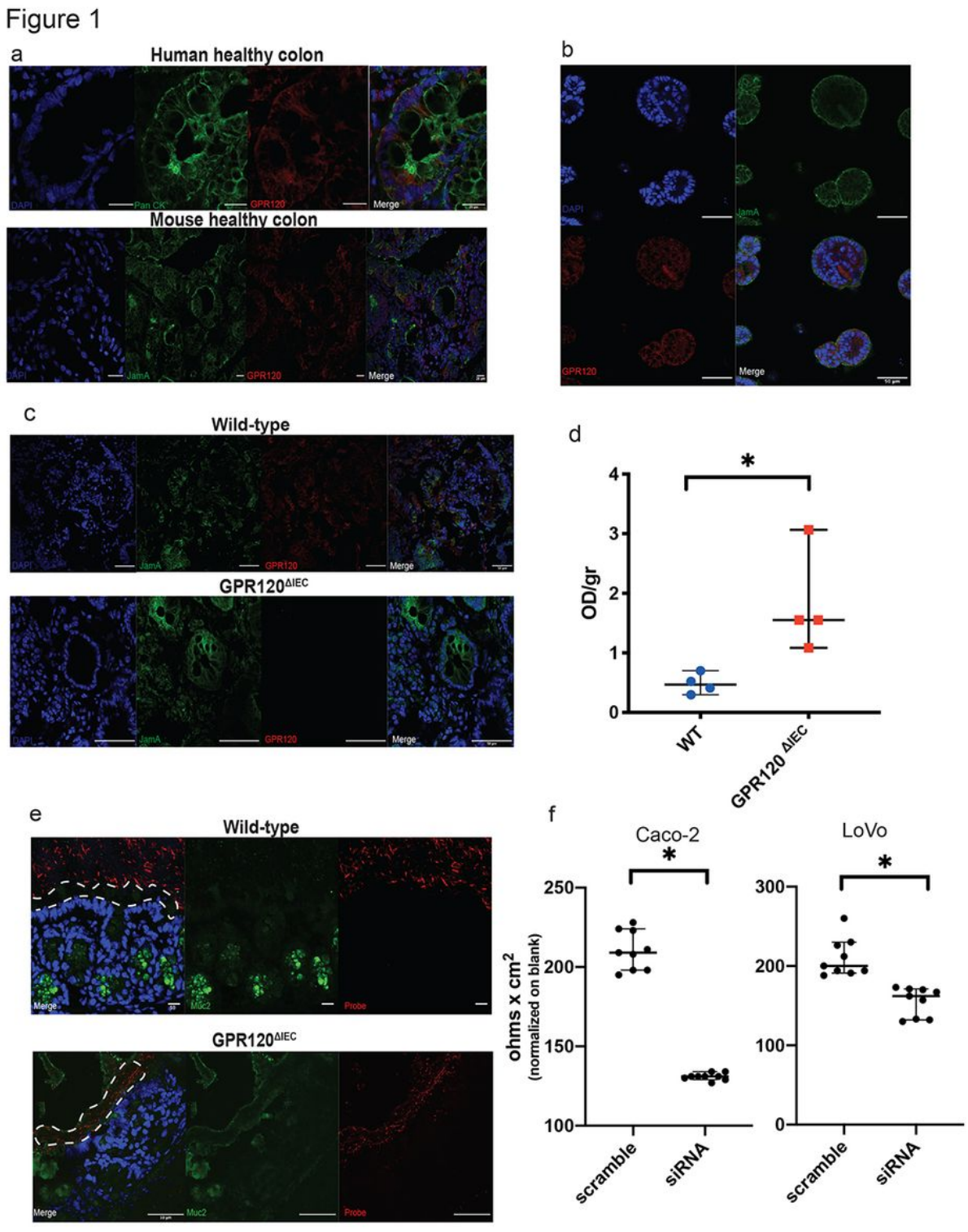

Figure 1

"Please see the Manuscript PDF file for the complete figure caption".

Figure 2

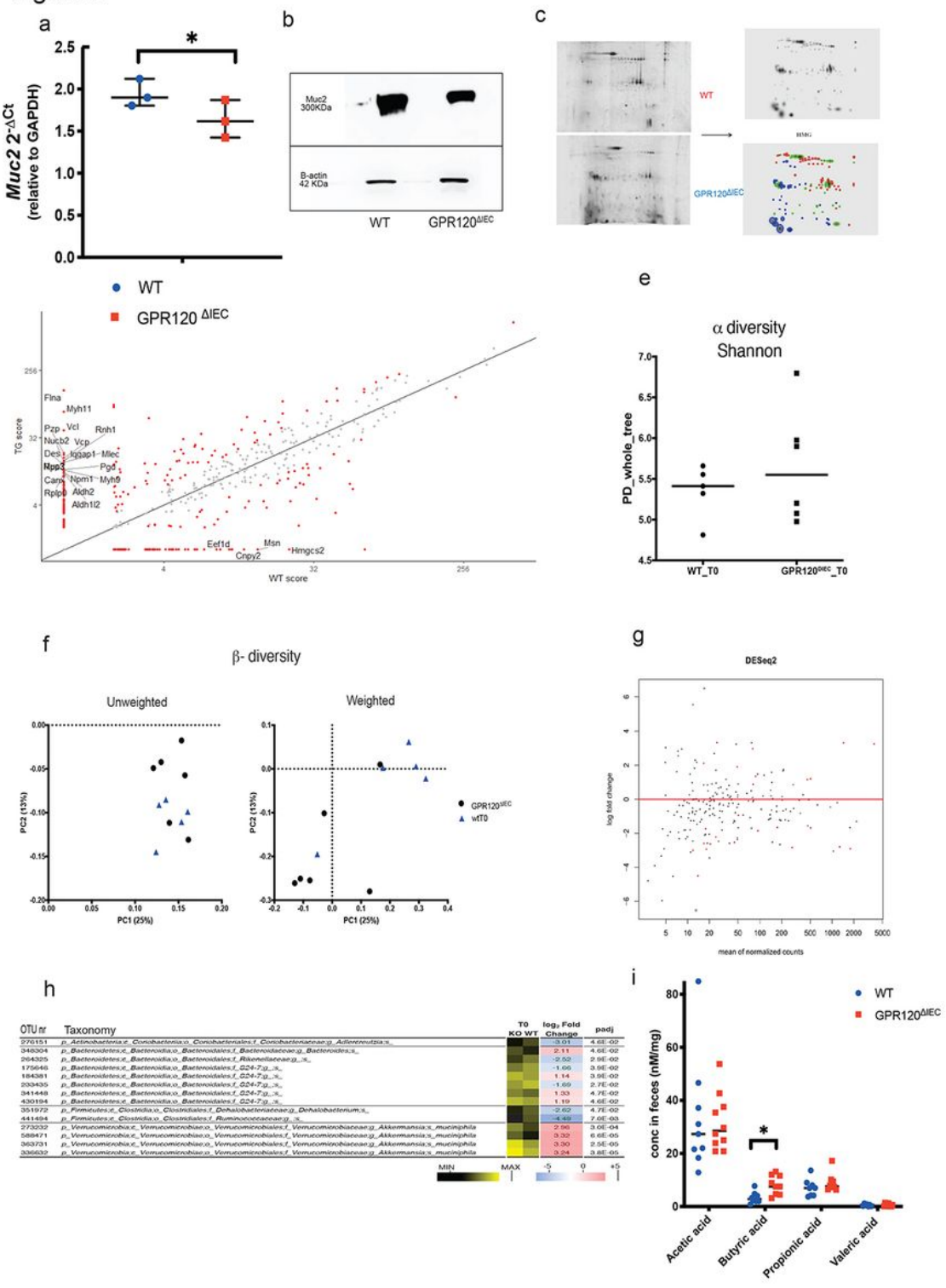

Figure 2

"Please see the Manuscript PDF file for the complete figure caption".

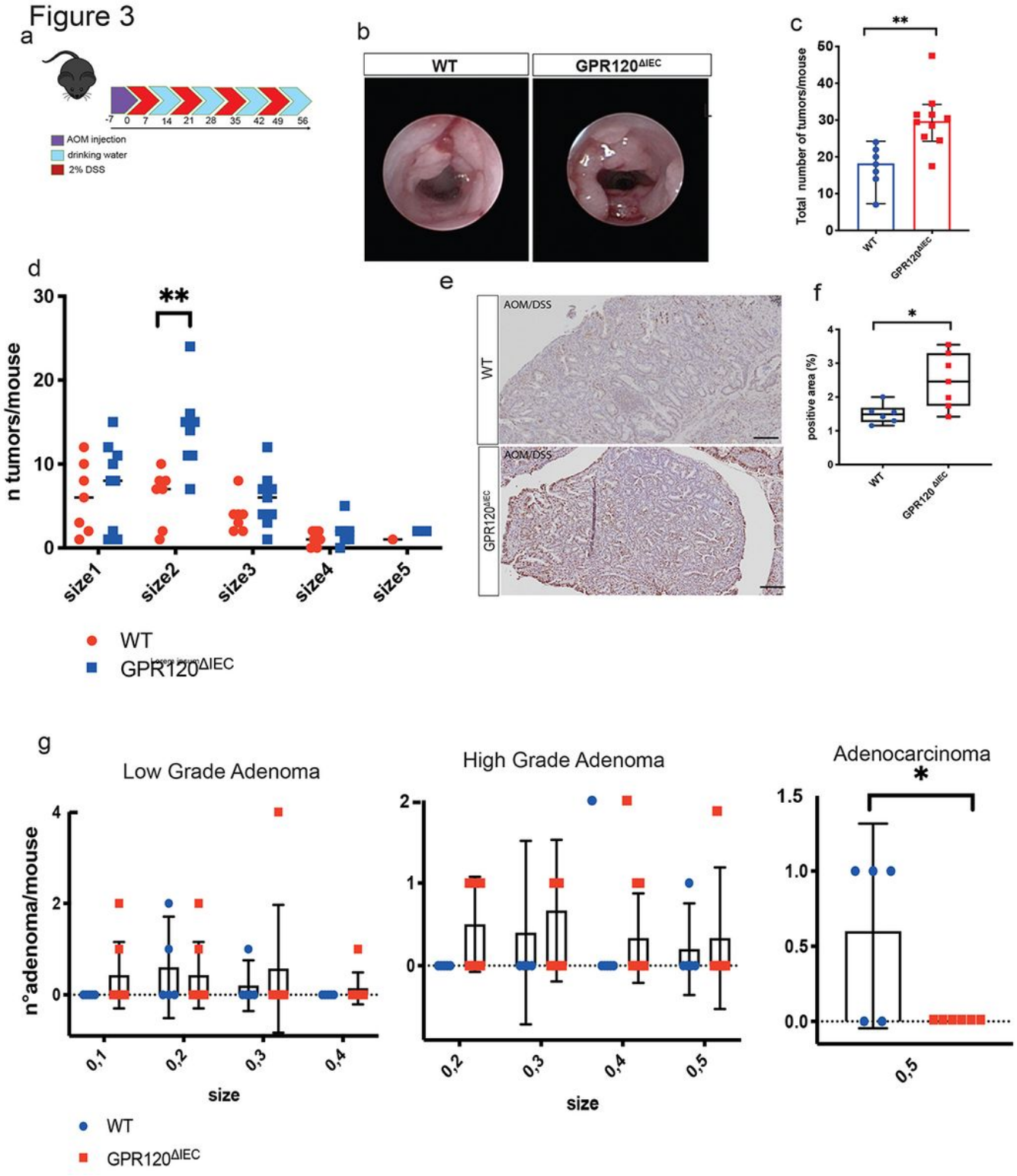

Figure 3

"Please see the Manuscript PDF file for the complete figure caption".

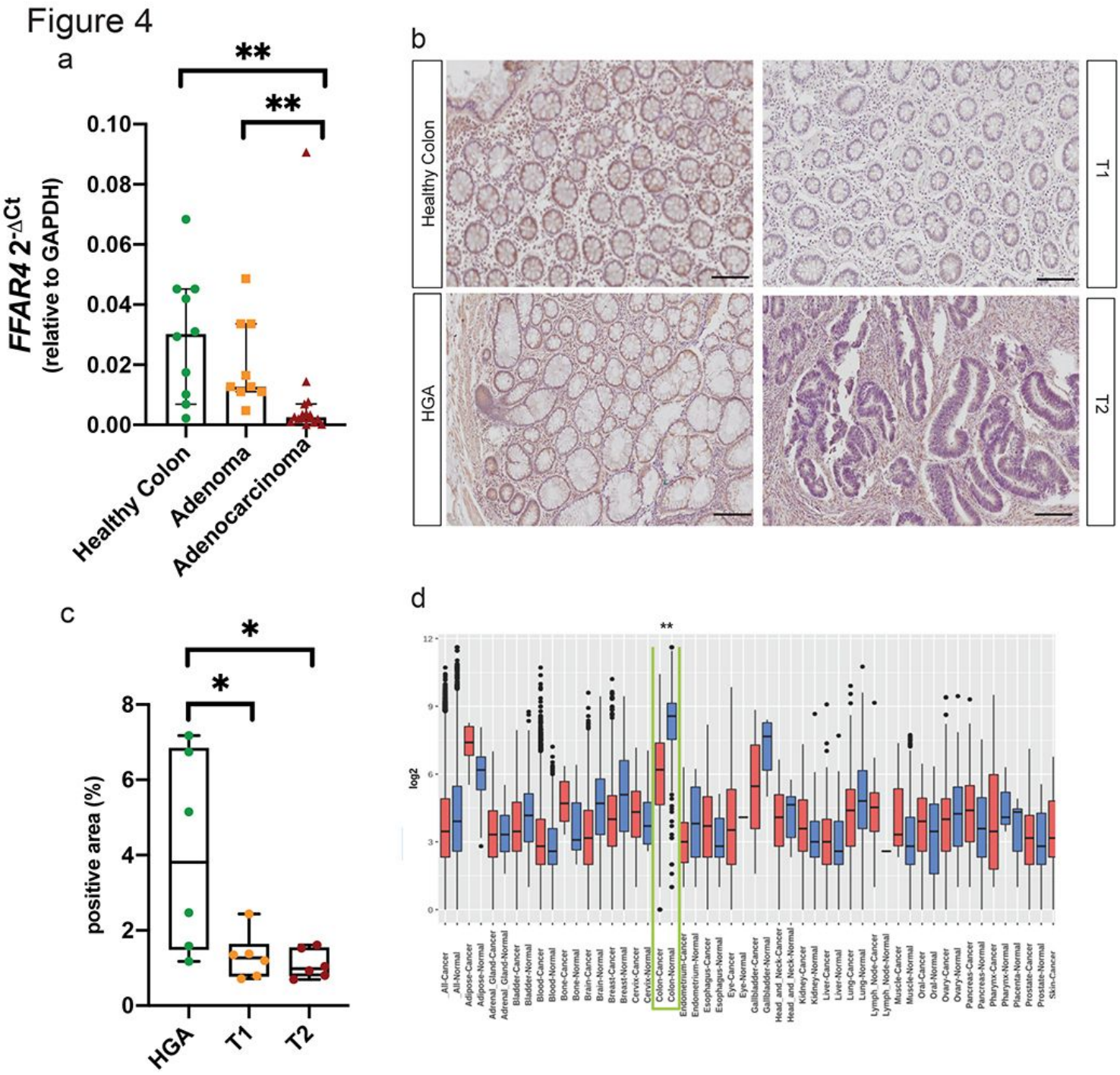

Figure 4

"Please see the Manuscript PDF file for the complete figure caption".

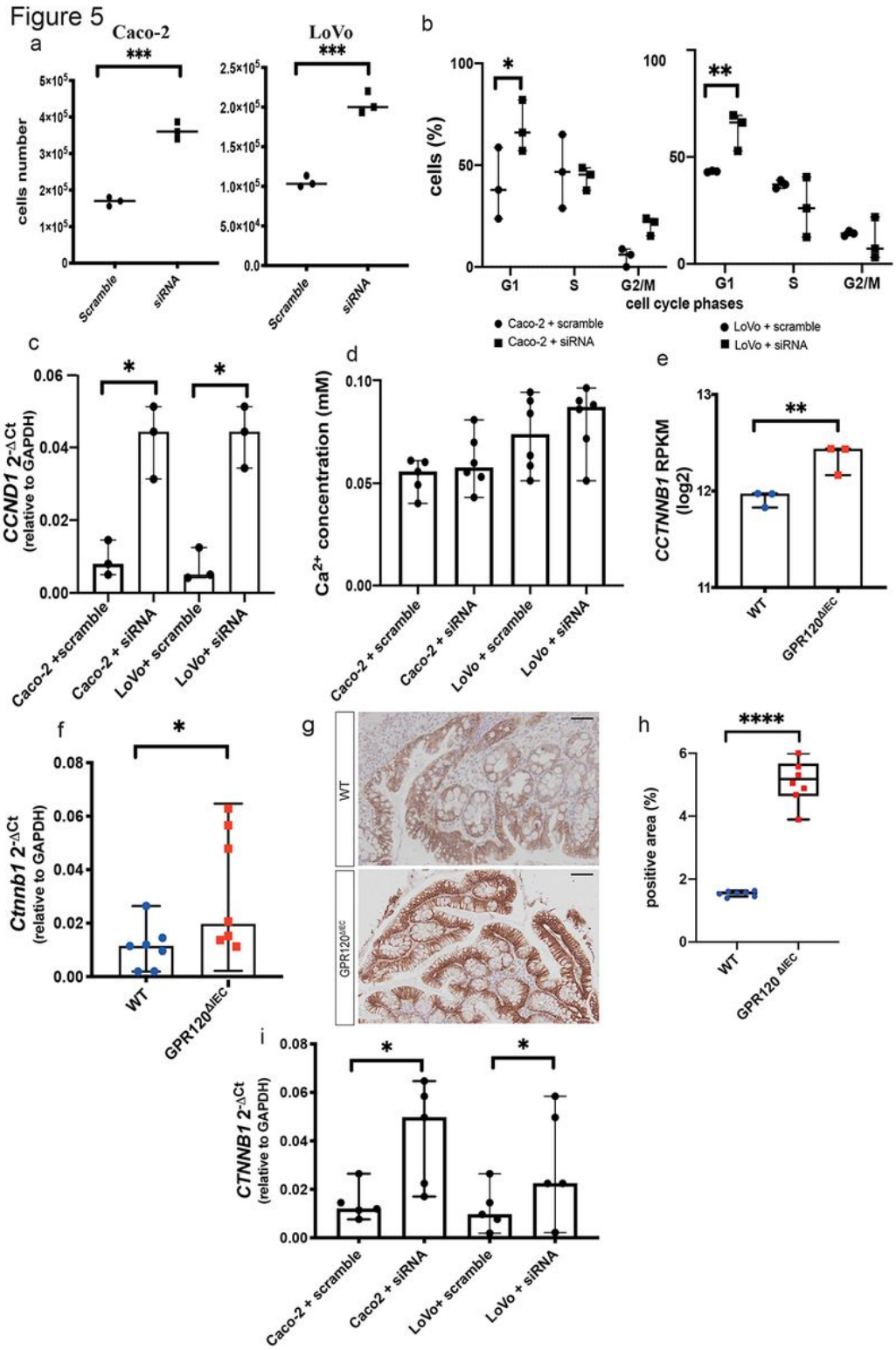

Figure 5

"Please see the Manuscript PDF file for the complete figure caption".

Figure 6

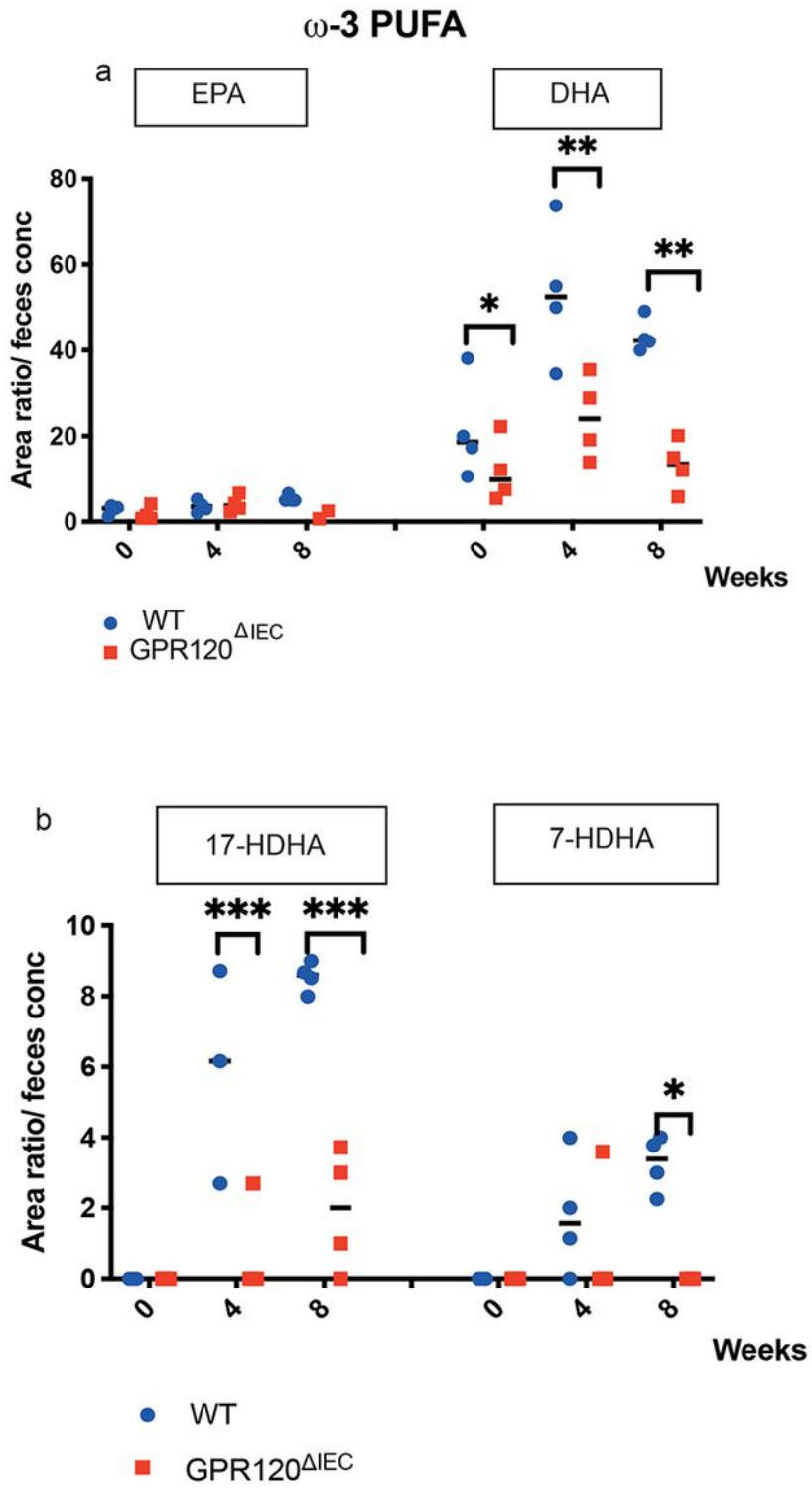

Figure 6

"Please see the Manuscript PDF file for the complete figure caption".

Supplementary Files

This is a list of supplementary files associated with this preprint. Click to download.

- ARRIVEstatement.pdf
- pdf24merged3.pdf